Finite-difference Time-domain Studies of the Optical Properties of Nanoshell Dimers

C. Oubre† and P. Nordlander*

Department of Physics and Department of Electrical and Computer Engineering, Rice Quantum Institute, M.S. 61, Rice University, Houston, Texas 77251-1892

Received: December 9, 2004; In Final Form: March 15, 2005

The optical properties of metallic nanoshell dimers are investigated using the finite difference time domain (FDTD) method. We discuss issues of numerical convergence specific for the dimer system. We present results for both homodimers and heterodimers. The results show that retardation effects must be taken into account for an accurate description of realistic size nanoparticle dimers. The optical properties of the nanoshell dimer are found to be strongly polarization dependent. Maximal coupling between the nanoshells in a dimer occurs when the electric field of the incident pulse is aligned parallel to the dimer axis. The wavelengths of the peaks in the extinction cross section of the dimer are shown to vary by more than 100 nm, depending on the incident electric field polarization. The calculations show that electric field enhancements in the dimer junctions depend strongly on dimer separation. The maximum field enhancements occur in the dimer junction and at the expense of a reduced electric field enhancement in other regions of space. We investigate the usefulness of nanoshell dimers substrates for SERS by integrating the fourth power of the electric field enhancements around the surfaces of the nanoparticles as a function of dimer separation and wavelength. The SERS efficiency is shown to depend strongly on dimer separation but much weaker than the fourth power of the maximum electric field enhancement at a particular point. The SERS efficiency is also found to depend strongly on the wavelength of the incident light. Maximum SERS efficiency occurs for resonant excitation of the dimer plasmons.

I. Introduction

There has been much research in recent years on tailoring the plasmonic properties of nanostructures for use as substrates in surface-enhanced spectroscopies such as surface-enhanced Raman spectroscopy (SERS).[1,2] The physical mechanism underlying the surface-enhanced cross sections in these spectroscopies is excitation of surface plasmons. The plasmons can induce large local electromagnetic fields in the vicinity of the surfaces of the nanoparticles. In the case of SERS, the cross section depends on the square of the electric field intensities at the incident and shifted wavelengths and can thus be strongly enhanced by excitation of surface plasmons. The effect is particularly pronounced when the wavelength of the incident and shifted radiation are near resonant with a plasmon energy of the substrate. In this case, the cross section can depend on the fourth power of the induced electric field strength across the target molecule.

For the rational design of nanostructures capable of providing strong enhancements for surface-enhanced spectroscopies, one must consider both optimizing the electric field enhancements associated with the surface plasmons and, equally important, optimizing the wavelength of the surface plasmon resonance so the enhancements occur at a wavelength where the target molecules are Raman active.

Giant SERS enhancements of around twelve orders of magnitude have been reported for aggregates of colloids.[3−6] However, because of the lack of tunability of this type of substrate, its effectiveness is limited to a narrow band of wavelengths not necessarily relevant for SERS. Additionally, the large electric field enhancements are located at a few random "hot spots" in the aggregates,[7,8] making the systematic design of an efficient SERS substrate with a large active surface area difficult.

The electromagnetic field enhancements associated with nanoparticle plasmons depend to a large extent of nanoparticle shape and structure.[9] The electromagnetic field enhancements associated with dipolar plasmons in spherical nanoparticle typically linger around an order of magnitude. For more complex nanostructures, i.e., dimers or trimers, the enhancements in their junctions at wavelengths resonant with a plasmon mode can be as large as 3 orders of magnitude.[10]

The importance of nanoparticle dimers in the context of surface-enhanced Raman spectroscopy was recognized long ago.[11] Since then, a large number of theoretical and experimental studies of the nanoparticle dimer system have been performed.[12−21] Although nanoparticle dimers clearly are not the optimal substrate structure for SERS, they serve as a simple prototypical model system for the study of the important physical factors underlying the electromagnetic field enhancements. The two major factors are the interaction of localized plasmons and the interference of the electromagnetic fields generated by these plasmons.

A particularly useful nanoparticle in SERS applications is the metallic nanoshell.[22,23] A nanoshell consists of a small dielectric core, usually silica, surrounded by a thin layer of a noble metal, such as silver or gold.[24] The plasmon resonance of nanoshells is tunable from wavelengths in the mid-infrared to the visible region of the spectrum.[25,26] The unique tunability of metallic nanoshells offers the opportunity of placing the plasmon resonances at a wavelength desired for a particular

* Author to whom correspondence should be addressed. E-mail: nordland@rice.edu. Visit http://cmt.rice.edu.
† E-mail: coubre@rice.edu.

10.1021/jp044382x CCC: $30.25
Published on Web 04/26/2005

SERS application. While the plasmonic properties of individual nanoshell particles are well understood,[27−30] no studies have yet been performed on the optical properties of nanoshell dimers.

In this paper, we present a detailed theoretical investigation of the optical properties of metallic nanoshell dimers. The calculations are made using a recently developed finite difference time domain (FDTD) method.[31] The investigation shows that, as two nanoshells are brought close to each other, dimer plasmons are formed by hybridization of individual nanoshell plasmons. The situation is qualitatively similar to what was found in a recent study of the plasmonic properties of solid nanosphere dimers.[32] For large dimer separations, the interaction between the two nanoshells is dominated by a dipolar interaction. The individual nanoshell dipolar plasmons interact and form bonding and antibonding dimer plasmons that red-shift and blue-shift as a function of dimer separation. As the dimer separation is decreased, higher angular momentum plasmons begin to mix with the dipolar plasmons, resulting in several dipole-active dimer plasmons. We calculate the extinction cross sections and near-field properties of the dimer as a function of dimer separation, wavelength, and incident light polarization. We show that retardation effects play an important role both for the far-field spectra and, in particular, for the near-field electric field enhancements. Both the maximum electric field enhancements and their spatial locations are found to depend strongly on wavelength and polarization of the incident light. The maximum electric field enhancement in the junction between two closely separated nanoshells is found to be around an order of magnitude larger than the maximum electric field enhancement for a single nanoshell. These strong electric field enhancements are localized to a relatively small volume in the region between the two nanoshells. The strong electric field enhancements in the dimer junction are induced at the expense of a reduced field enhancement in other regions of space around the dimer. We investigate the efficiency of nanoshell dimers for SERS by integrating the fourth power of the electric field enhancement around the surface of the individual nanoshells as a function of wavelength and dimer separation. The SERS efficiency of the dimer is found to be strongly dependent on dimer separation, but considerably less so than the fourth power of the maximum electric field enhancements. The SERS efficiency of the dimer system is also found to be strongly dependent on the wavelength of the incident light. Maximum SERS efficiency occurs for resonant excitation of the dimer plasmons. For incident light tuned to the dimer plasmon resonance, the maximum SERS efficiency at close dimer separations is found to be around 3 orders of magnitude larger than the maximum SERS efficiency of two individual nanoshells.

The results of this investigation show that nanoshell dimers offer the same strong local field enhancements in their junctions as are found in the junctions of other types of metallic nanoparticle dimers. A distinct advantage with the nanoshell system is that the wavelength at which the maximum enhancement occurs can be tuned simply by varying the core−shell ratio of the individual nanoshells.

The organization of this paper is as follows. In section 2, we will briefly discuss the FDTD method, including specific numerical considerations appropriate for the dimer system. In section 3, the method will be applied to several different nanoshell dimer systems. Specifically, in sections 3.1 and 3.2, we discuss the far- and near-field properties of the homodimer. In sections 3.3 and 3.4, we discuss the far- and near-field properties of the heterodimer. In section 4, we discuss the relevance of our results for SERS and, in particular, the calculations of the integrated fourth power of the electrical field enhancements as a function of wavelength and dimer separations.

II. The FDTD Method

A. General Overview. There are many methods available for modeling the optical response of nanoparticles in both the near- and far-field regions.[33]

The calculations in this paper are made using the finite difference time domain (FDTD) method.[34,35] The method is an explicit time-marching algorithm used to solve Maxwell's curl equations on a discretized spatial grid. We have recently developed an efficient implementation of this method suitable for execution on distributed memory architectures.[31] To avoid repetition, the reader is referred to this reference for specific details on our FDTD implementation.

A dielectric function $\epsilon(\vec{r},\omega)$ is used to simulate materials in the grid. The values for ϵ are specified at every grid point. To model a nanostructure of a particular material, the grid points within that structure are each assigned appropriate dielectric parameters. To simulate gold and silver nanoshells, we implemented a Drude-like dielectric function of the following form

$$\epsilon(\omega) = \epsilon_\infty - \frac{\omega_p^2}{\omega^2 + i\delta\omega} \tag{1}$$

The parameters are obtained by fitting this dielectric function to a particular frequency range of bulk dielectric data[36] for the metal under study. We found that for silver from 400 to 1200 nm, the values of $\epsilon_\infty = 5.0$, $\omega_p = 9.5$ eV, and $\delta = 0.0987$ eV give a reasonable fit to the bulk dielectric data. Recent experimental results from dark-field spectroscopy of individual nanoshells suggest that no additional broadening needs to be added to δ in the dielectric function.[37]

To denote the geometry of the nanoshells, we adopt a notation (a, b), where a is the inner radius and b is the outer radius of the metallic shell. The material of the nanoshell core is taken to be silica with a dielectric constant of 2.08. The plasmon energies of an individual nanoshell is a function of its aspect ratio $x = a/b$.[25] For each angular momentum l and orientation m, there are two plasmon resonances $\omega_{l\mp}$ corresponding to symmetric or antisymmetric alignment of the multipole moments of the primitive plasmons associated with the inner surface (cavity plasmon) and outer surface (sphere plasmons) of the shell.[27] The splitting of these plasmon modes depend on the aspect ratio of the nanoshell. In the present study we will consider nanoshells with such large aspect ratios ($x = 0.81$) that the ω_{l+} modes will lie well above the energies of the lowest dimer plasmons and, therefore, play no significant role in the optical properties of nanoshell dimers for longer wavelengths than 400 nm.

B. Numerical Considerations. In this section we present numerical considerations one must take into account when using the FDTD method for the dimer geometry. The principal numerical obstacle in an FDTD calculation involving spherical particles is staircasing errors. These errors arise from trying to describe curved surfaces on a Cartesian grid. The actual surface of the nanoparticles will be built up by square discontinuous blocks. The numerical error introduced by staircasing vanishes only linearly with mesh size. In previous investigations of the optical properties of individual nanoshells, we have shown that these discretization errors introduce a slight blue-shift in the location of the plasmon peak in the extinction spectra calculated

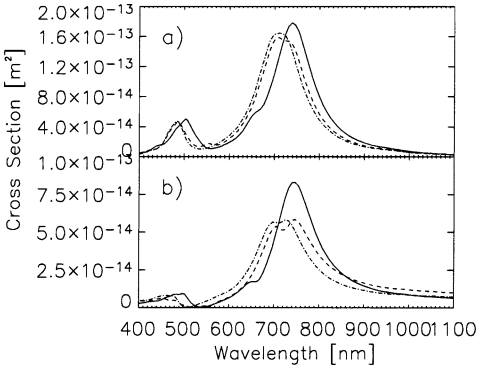

Figure 1. Extinction cross section (a) and scattering cross section (b) of a (39,48) nm Ag homodimer with dimer separation 1.5 nm for various mesh resolutions. The solid curve denotes a mesh size of 1.5 nm, the dashed curve, 0.75 nm; dot−dashed curve 0.5 nm mesh size. The polarization of the incident wave is parallel to the dimer axis. Note that the scale of the extinction and scattering cross sections are different in (a) and (b).

by the FDTD method.[31,38] The error vanishes with decreasing mesh resolution.

Figure 1 illustrates another pitfall one may encounter using the FDTD method, the appearance of spurious peaks in the calculated extinction cross section spectra. In the following, we will refer to these peaks as "ghost" peaks. In the upper part of Figure 1, we plot the extinction cross section for a (39, 48) nm nanoshell homo dimer at different mesh resolutions. The two major features are the two bonding dimer plasmons derived from the dipole and quadrupole resonances of the individual nanoshells.[32] As expected, the plasmon resonances shift to higher energies with increasing mesh resolution. However, for the coarsest resolution, the extinction spectrum exhibits a weak feature at 650 nm. As the resolution is increased, this feature red-shifts and eventually merges with the dipolar dimer plasmon resonance. To analyze the origin of the ghost peak, we calculated the absorption and scattering cross section of the systems separately. The absorption spectrum that gives the dominant contribution to the extinction was found to be almost identical for all grid resolutions. Only the scattering spectrum exhibited the ghost peak. In the lower panel of Figure 1, we show the scattering spectrum of the system. The spectra clearly reveal the ghost peak and its sensitivity to grid resolution. As the resolution increases, this ghost peak approaches the dipole peak, resulting in a double-peaked structure. The ghost peaks do not appear to significantly change the overall shape of the spectra. An analysis using the plasmon hybridization method[39] suggests that the "ghost" peaks are nonphysical. With finer mesh resolutions, the ghost peaks are eliminated. In our numerical investigations of this effect, we have found that the ghost peaks typically become negligible if the mesh size is small enough to allow 4−5 grid cells between the two nanoparticles. The physical origin of the ghost peak is a multiple scattering event against the staircased surfaces of the nanoshell dimer junction.

In Figure 2, we show the convergence of the near-field enhancements in the center of a homodimer as a function of mesh size for two different dimer separations. As is the case for individual nanoshells,[31] the electromagnetic field enhancements for a coarse mesh tend to underestimate the actual electric field enhancements, and quick calculations using large mesh sizes can be used to set lower bounds on the near-field enhancements. Figure 2 shows that the electric field enhancements for a dimer separation of $D = 1.5$ nm are not completely converged for the smallest mesh sizes that can be used with the present computational resources. However, for a dimer

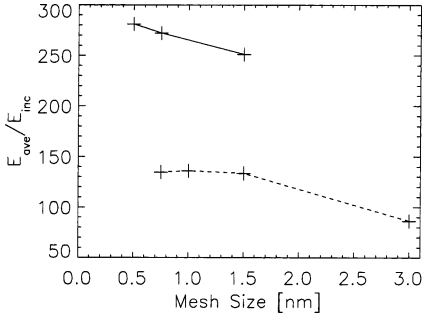

Figure 2. Convergence of calculated electric field enhancements in the junction of a nanoshell dimer for different dimer separations. The upper curve (solid line) shows the average field enhancements in a 1.5 nm^3 volume centered at the midpoint of the dimer axis for $D = 1.5$ nm, and the lower curve (dashed line) shows the average electric field enhancements in 3 nm^3 volume for $D = 3$ nm. The homodimers analyzed were comprised of (39,48) nm Ag nanoshells with silica cores. The incident pulse is polarized parallel to the dimer axis (polarization A as defined in Figure 3 and text).

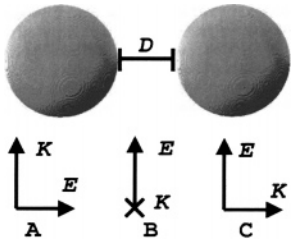

Figure 3. The coordinate system and the three optical polarization and propagation orientation combinations used in the calculations throughout this paper. D is the dimer separation measured from the two nearest surfaces of the nanoshells.

separation of $D = 3.0$ nm, the calculations converge satisfactorily for a mesh size of 1.5 nm. Throughout this paper, we will limit ourselves to dimer separations $D \geq 3$ nm and use a mesh size of 0.75 nm, which is also sufficiently small to prevent the appearance of ghost peaks.

The staircasing can result in unphysical strong local electric field enhancements at the surfaces of the nanoparticles. These electric field enhancements will show up as very bright spots in the color contour plots of the electric field enhancements that will be presented below. The spatial extent of these hot spots is only a grid cell. In practice, it is very easy to identify and discard these spots. In the following, when we show electromagnetic field enhancements at particular positions, we consider only positions sufficiently far from staircased corners that the influence of these hot spots is negligible.

III. Results

In the following section, we present calculations of the far-field and near-field response for a homodimer, a dimer of two similar nanoshells, and a heterodimer, a dimer of two different nanoshells. All of the systems we study are assumed to be in a vacuum. We use three different polarizations of incident illumination, shown in Figure 3, to study these systems. Polarization A is defined as the electric field and is polarized along the dimer axis. Polarization B represents both the electric field polarization and propagation vector perpendicular to the dimer axis, and polarization C denotes electric field polarization perpendicular to the dimer axis and propagation parallel to the dimer axis. The polar axis for the dimer is chosen along the dimer axis. The azimuthal number m denotes the orientation of the plasmons. Plasmons polarized along the dimer axis have $m = 0$, and plasmons polarized perpendicular to the dimer axis

have $m = \pm 1$. In the quasistatic limit, a light wave with A-polarization would only excite dimer plasmons with $m = 0$, and incident waves with B- and C-polarizations would only excite $m = \pm 1$ plasmons.

To facilitate the discussion of the results to be presented in this paper, we end this subsection with a brief discussion of the microscopic properties of dimer plasmons.

The nature of plasmon resonances in nanoparticle dimers was recently elaborated using the plasmon hybridization approach.[32] The dimer plasmons can be viewed as formed by interactions of the plasmons on the individual nanoparticles. A plasmon of a given angular momentum l and orientation m on one of the nanoparticles will interact with all plasmons of the same orientation on the other nanoparticle. Thus, the dimer plasmons will not have a well-defined angular momentum but contain an admixture of individual nanoparticle plasmons of different angular momenta. For large dimer separation, the interaction between the individual nanoshell plasmons is weak. Because the energies of the individual nanoparticle plasmons depend on their angular momentum, the dimer plasmons are simply bonding and antibonding combinations of individual nanoparticle plasmons of the same angular momentum l. For smaller dimer separations where the interactions between the different individual nanoparticle plasmons becomes comparable to their energy differences, the dimer plasmons contain a finite admixture of individual nanoparticle plasmons of all angular momenta l. The significant admixture of individual dipolar nanoshell plasmons into many of the dimer plasmons allows them to couple more strongly to an incident light wave. For this reason, as the dimer separation becomes smaller, additional peaks will appear in their extinction spectra. We will refer to the dimer plasmons using their asymptotic angular momentum, i.e., the angular momentum of the dimer plasmons in the limit of infinite dimer separation. We emphasize that the notation refers to the asymptotic limit! For finite nanoparticle separation, all l dimer plasmons will contain a finite admixture of individual nanoparticle plasmons of all angular momenta, including the individual dipolar nanoparticle plasmons that couple efficiently to light.

A. Homodimer Far Field. In Figure 4, the extinction cross section for a (39,48) nm silver homodimer for two dimer separations and the three different polarizations is shown. Because the incident light wave for these relatively small systems is mostly dipolar, the peaks seen in Figure 4 are the plasmons that have the largest dipole moment.

Maximal coupling between the nanoshells occurs when the electric field of the incident pulse is aligned parallel to the dimer axis, configuration A in Figure 3. For a dimer separation of $D = 19.5$ nm, the extinction spectrum is characterized by a bonding $l = 1$ dimer plasmon at 593 nm and a weak bonding $l = 2$ plasmon at 485 nm. The dimer plasmon energies are red-shifted compared to that of the individual nanoshell plasmons at 543 and 440 nm. For a dimer separation of $D = 3.0$ nm, we see two pronounced features at 677 and 464 nm. These resonances correspond to the $l = 1$ and 2 dimer plasmons. The intensity of the $l = 2$ dimer plasmon is significant because of the increased admixture of the individual nanoshell dipolar plasmon at this smaller dimer separation. The figure also shows that the red-shift of the $l = 1$ plasmon with decreasing dimer separation is larger than that for the $l = 2$ plasmon. This finding is consistent with the previous investigation of solid-sphere dimers and is caused by the fact that the interaction between the individual $l = 2$ plasmons is weaker.[32] For all dimer separations under A-polarization excitation, the observed values

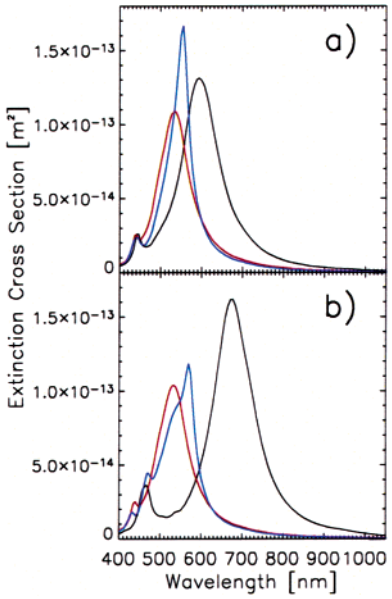

Figure 4. The extinction cross section of a (39,48) nm Ag homodimer for various separation distances and polarizations. The three polarizations, as defined in Figure 3, are A (black), B (red), and C (blue). Dimer separations: (a), 19.5 nm; (b) 3.0 nm.

for the plasmon locations are red-shifted from the corresponding single-nanoshell plasmons. This is indicative of bonding configurations, i.e., the charge oscillations on both shells are in phase with each other.[32] This configuration provides the largest dipole moment and the lowest energy. We will refer to the bonding dimer plasmons as "bright" in contrast to the "dark" antibonding plasmon, with the dipole moments of the individual nanoshells aligned opposite to each other.

Considerably less coupling occurs when both the pulse polarization and the direction of propagation are perpendicular to the dimer axis, B-polarization in Figure 3. This case corresponds to a symmetric excitation of plasmons perpendicular to the dimer axis, i.e., antibonding $m = 1$ dimer plasmons. The figure shows that the extinction spectra for the two dimer separations are very similar. Two features at 533 and 439 nm are visible. These correspond to the antibonding $l = 1$ and $l = 2$ dimer plasmons, respectively. Both of these plasmon resonances are blue-shifted compared to that of the individual nanoshell plasmons. The reason for the blue-shift is that, for the homodimer for $m = 1$, it is the antibonding dimer plasmons that have their dipole moments aligned.[32] The bonding $m = 1$ plasmons are not visible because the dipole moments of the individual nanoshells are out of phase.

A very interesting situation occurs when the incident light is polarized perpendicular to the dimer axis and incident along the dimer axis (configuration C in Figure 3). In this situation, retardation effects are enhanced and the symmetry of the excitation process is broken. An incident light wave can now excite both the bonding and antibonding $m = 1$ dimer plasmons. For the large dimer separation $D = 19.5$ *nm*, the extinction spectra reveals an asymmetric feature around 555 nm. This feature consists of the bonding and antibonding $l = 1$ dimer resonances. Because of the weak interaction for large dimer separations, the difference in energy between these modes is smaller than their widths, preventing the clear resolution of the two different dimer plasmon modes. For the smaller dimer separation $D = 3.0$ nm, where the energy differences between bonding and antibonding dimer plasmons are larger, we observe four plasmon peaks at 568, 533, 468, and 431 nm, corresponding

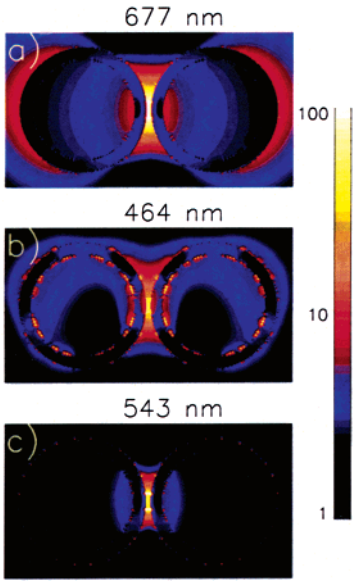

Figure 5. Color contour plot of the near-field distributions for a (39,-48) nm Ag nanoshell homodimer at wavelengths corresponding to excitations of the specific bright bonding dimer plasmons $l = 1-3$ observed in Figure 4 for an incident wave of A-polarization. The bottom panel shows the field distribution for a wavelength corresponding to the $l = 1$ plasmon of an individual nanoshell. The dimer separation is 3.0 nm. The maximum enhancements for the different wavelengths are 136 (677 nm), 50 (464 nm), and 53 (543 nm).

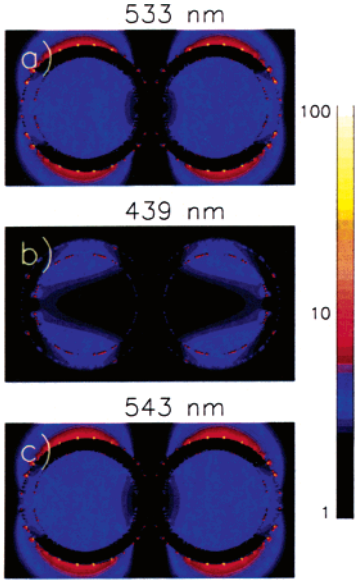

Figure 6. A color contour plot of the near-field distributions and electric field enhancements for a (39,48) nm Ag nanoshell homodimer for the wavelengths corresponding to excitations of the specific bright bonding dimer plasmons $l = 1-2$ observed in Figure 4 for an incident wave of B-polarization. The bottom panel shows the electric field enhancement for a wavelength corresponding to the $l = 1$ plasmon of an individual nanoshell. The dimer separation is 3.0 nm. The maximum enhanvements for the different wavelengths are 8 (533 nm), 4 (439 nm), and 8 (543 nm).

to both the bonding and antibonding configurations of the $m = 1$, $l = 1$ and 2 plasmons.

B. Homodimer Near Field. In this section, we present near-field calculations for the field distributions of the (39,48) nm silver homodimer with a dimer separation of $D = 3.0$ nm. We define electric field enhancement as the ratio of the actual electric field strength to incident electric field strength. Figure 5 shows the wavelength dependence of the spatial distribution of the electric field enhancements in the near-field region of a silver homodimer illuminated by light with A-polarization. The different panels show the electric field enhancements for the wavelengths corresponding to the different extinction maxima. We also include the electric field enhancements for a wavelength corresponding to the $l = 1$ plasmon of an individual nanoshell.

When the electric field is polarized parallel to the dimer axis, the maximum of the near-field enhancements is focused between the nanoshells. The plasmon modes of each of the nanoshells are aligned, inducing a large electric field across the junction. On the surfaces on either end of the dimer, we also see an area of enhancement similar in magnitude and extent to the electric field enhancement of the individual nanoshell.[31] The maximum field enhancement is found at the wavelength corresponding to the excitation of the $l = 1$ dimer plasmon resonance, which for this polarization is 136. For this polarization, the average enhancement within a 34-cubic-nanometer strip located in the interparticle junction of the dimer in plane with the incident electric field is 134. For the three longest wavelengths, the maximum enhancement occurs on the dimer axis. For the shortest wavelength, the maximum field enhancement occurs in a region that is slightly outside the dimer axis. The figure clearly shows that the electric field enhancements are largest for resonant excitation of the dimer plasmons.

Figure 6 shows the near-field distribution and the electric field enhancements of the same nanoshell dimer as in Figure 5 following illumination of light with B-polarization. The plots show that the coupling between the plasmons in the individual nanoshell is very small. In this case, the electric field enhancements are essentially superpositions of the field enhancements of the individual nanoshells. As stated in section 3.1, for light with B-polarization, the plasmon modes of each nanoshell of the dimer are aligned. For this reason, no electric fields are induced along the dimer axis. Figure 6 clearly shows that the electric field enhancements in the dimer junction are very small. The maximum field enhancement associated with the excitation of the $l = 1$ dimer plasmon for B-polarization is only 8 and occur at the top and bottom of each nanoshell. The figure also illustrates the wavelength dependence of the electric field enhancements. For 439 nm corresponding to the excitation of the dimer $l = 2$ plasmon, the electric field enhancements are very small because of the weak coupling of this dimer plasmon with the incident light. Also for this polarization, the electric field enhancements are largest near the resonant excitation of the dimer plasmons, in agreement with experimental measurements.[22,23]

In Figure 7, we show the near-field distributions and electric field enhancements of the same dimer as discussed in Figures 5 and 6, illuminated with C-polarized light, i.e., the $\vec{k}$ vector of the incident wave, is now parallel to the dimer axis. For this polarization, an asymmetric near-field distribution is observed. The light wave is incident from the left, and we see that the electric field enhancements are concentrated around the left-most nanoshell. As mentioned in the previous subsection, for C-polarization, retardation effects (finite speed of light) will lead to excitation of both the bonding (dark) and antibonding (bright) dimer plasmons. The bonding dimer plasmons with the dipole moments of each nanoparticle aligned in opposite directions will induce a large field across the junction between the nanoparticles and give rise to significant field enhancement in the region of the junction. The antibonding dimer plasmons with the symmetric alignment of dipole moments in adjacent nanoparticles does not cause significant field enhancement in the junction as is also seen in Figure 6. The maximum field enhancement

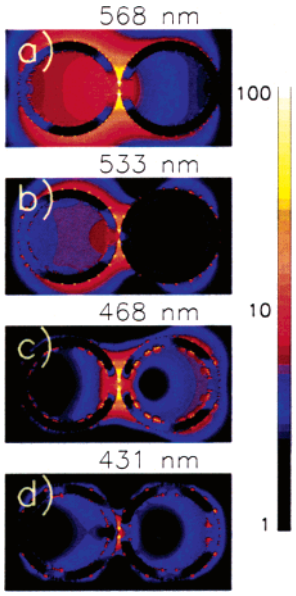

Figure 7. This figure plots the near-field enhancements for a (39,48) nm silver nanoshell homodimer for an incident electromagnetic wave with C-polarization. The wavelengths correspond to excitations of the bonding and antibonding $l = 1, 2$ dimer plasmons. The dimer separation is 3.0 nm. The maximum enhancements for the different wavelengths are 62 (568 nm), 31 (533 nm), 61 (468 nm), 19 (431 nm), and 35 (543 nm).

following excitation of the bonding $l = 1$ $m = 1$ dimer plasmon at its resonant wavelength of 568 nm is 62.

Figure 7 also shows that the spatial distributions of the maximum field enhancements for C-polarization depend strongly on the wavelength of the incident light. For A- and B-polarizations, only the magnitudes, not the spatial distributions, of the near-field enhancements for the homodimer change significantly with wavelength. This is not the case for C-polarization.

Figure 7 shows that, for a wavelength of 568 nm, the enhancement is concentrated around one of the nanoshells. For a wavelength of 468 nm, the regions of maximum field enhancements are shifted toward the other nanoshell. For 431 nm, the region of maximum field enhancement is symmetric in the junction. As was the case for A- and B-polarization, the largest field enhancements occur for resonant excitation of one of the dimer plasmons.

The field enhancements for light incident with C-polarization are not localized in the center of the junction. In Figure 8, we show the field enhancements as functions of position in the dimer junction for A and C-polarization. For A-polarization, the regions of maximum field enhancements are centered on the dimer axis. For C-polarization, the maximum enhancements are located around 8 nm away from the dimer axis. The sharp features seen in Figure 8 illustrate the effects of staircasing on the near-field enhancements. Even though the magnitude of these feature can be large, their spatial extent is roughly the size of one grid cell. This highly localized nature prevent the hot spots from greatly influencing the overall shape of the near-field enhancements. These features are representative examples of the hot spots seen in the near-field contour plots shown in this paper.

In Figure 9, we plot the field enhancement at specific spatial positions on our nanoshell dimer as a function of wavelength for the different polarization and propagation combinations being considered. For comparison, we also include the maximum field enhancement at a point outside an individual nanoshell. The

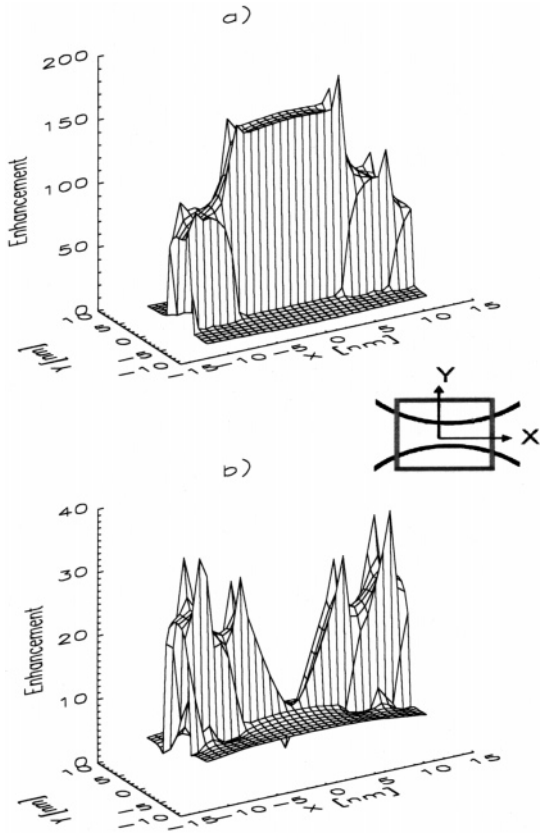

Figure 8. Near-field enhancements in the junction of a (39,48) nm Ag nanoshell homodimer with dimer separation $D = 3$ nm. Panel (a) is for A-polarization at 677 nm and panel (b) for C-polarization at 568 nm. Inset: the coordinate system is defined.

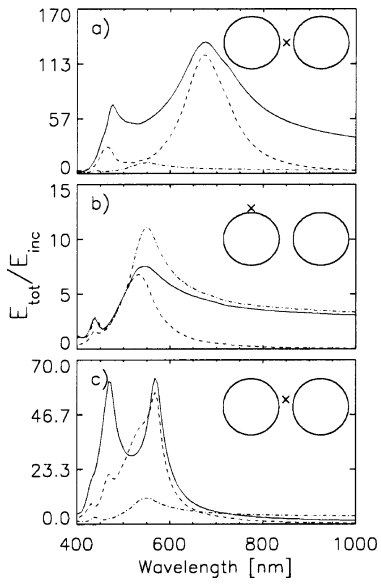

Figure 9. Maximum field enhancements (solid lines) at specific points on a nanoshell dimer as a function of wavelength for A-polarization (panel a), B-polarization (panel b) and C-polarization (panel c). Dashed lines are the corresponding extinction spectra. Dotted lines are the field enhancements at their maximal point outside an individual nanoshell. The dimer consists of two (39,48) Ag nanoshells with 3.0 nm separation. The positions points are illustrated in the insets. For A-polarization, the point is at the center of the dimer junction, for B-polarization, the point is on top of one of the nanoshells, and for C-polarization, the point is 7.5 nm from the dimer axis between the two nanoshells.

figures also include the extinction spectra for the dimer for the different polarizations. This figure clearly shows that the

maximum field enhancements follows the extinction cross sections of the dimer. The resonant excitation of any of the dimer plasmon modes thus translates into an increased field enhancement. The electric field enhancement peaks are broader than that of the corresponding extinction spectra. The long wavelength tails of the electric field enhancement curves are due to the nonresonant "lighting rod" effect.[30] In the near field, we observe the presence of a "ghost" peak as described in section 2.2.

For the A-polarization, the field enhancements are significantly larger than those outside an individual nanoshell for all wavelengths studied. The maximum field enhancement for excitation of the bonding $l = 1$ $m = 0$ and $l = 2$ $m = 0$ dimer plasmons are 136 and 50, respectively. The broad features around 450 nm correspond to the excitation of $l = 3$ $m = 0$ and higher-order l dimer plasmons. It is interesting to note that these plasmon modes are more clearly resolved in the field enhancement curves than in the extinction spectra.

The field enhancements for B-polarization are very similar to those of an individual nanoshell. This is due to the minimal coupling of the plasmon modes for this polarization. For C-polarization, the electric field enhancements are much larger than for that of an individual nanoshell because of the excitation of the dark bonding $m = 1$ dimer plasmons. These plasmons modes show up as strong peaks in the electric field enhancements. The electric field enhancements associated with excitation of the dark $m = 1$ $l = 1$ (568 nm) and $l = 2$ (468 nm) are 62 and 61, respectively. The weak feature at 432 nm corresponds to the dark $l = 3$ $m = 1$ mode. As in the case of A-polarization, the plot of electric field enhancements display the plasmon modes much more clearly than that of the extinction cross section.

C. Heterodimer Far Field. In this section, we investigate the optical properties of a heterodimer consisting of a nanoshell of geometry (39,48) nm and a second nanoshell of geometry (19.5,24) nm. This heterodimer is composed of nanoshells with the same aspect ratio, which in the electrostatic limit should be nanoparticles with the same plasmon resonance. However, because of phase retardation effects, the individual nanoshell plasmons are at different wavelengths. The smaller (19.5,24) nm nanoshell has its dipolar plasmon resonance at a wavelength of 524 nm and its quadrupole plasmon at 425 nm.

Figure 10 shows the extinction cross section of the heterodimer for two different dimer separations, 3.0 and 19.5 nm. The figure reveals the presence of more plasmon resonances than for the homodimer depicted in Figure 4. This is because the dipole moments of the individual nanoshell plasmons are different because the nanoshells differ in size. Thus, in this case, both the bonding and antibonding dimer plasmons will possess a net dipole moment.

For A-polarization ($m = 0$) and $D = 19.5$ nm in Figure 10a, three features are visible in the extinction spectra. The bonding $l = 1$ dimer plasmon is at 562 nm, the antibonding $l = 1$ dimer plasmon is at 502 nm, and the bonding $l = 2$ is at 440 nm. For a dimer separation $D = 3.0$ nm (Figure 10b), three features are visible, the bonding and antibonding $l = 1$ dimer plasmons at 618 and 509 nm, respectivley, and a broad feature at 451 corresponding to the bonding and antibonding $l = 2$ dimer plasmons.

For B-polarization ($m = 1$), at $D = 19.5$ nm, two features are clearly resolved, an asymmetric feature at 546 nm corresponding to the bonding and antibonding $l = 1$ dimer plasmons and the antibonding $l = 2$ plasmon at 439 nm. At this large dimer separation, the splitting between the antibonding and bonding plasmons are smaller than the widths of the plasmon resonances, making it difficult to resolve the bonding dimer plasmons. For the shorter dimer separation $D = 3.0$, three features are clearly visible, the bonding and antibonding $l = 1$ dimer plasmons at 553 and 528 nm, respectively, and the antibonding $l = 2$ dimer plasmons at 439 nm.

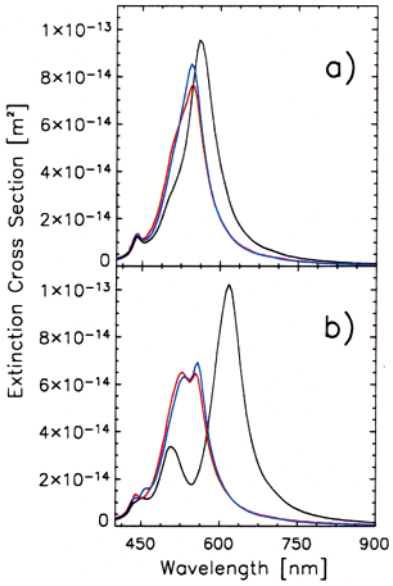

Figure 10. Extinction cross section for a heterodimer consisting of two Ag nanoshells of geometries (39,48) and (19.5,24) nm, respectively, at two different separation distances, illuminated with three different polarization propagation combinations considered. Panel (a) is for $D = 19.5$ nm and panel (b) is for $D = 3.0$ nm. The three polarizations as defined in Figure 3, are A (black), B (red), and C (blue).

In a fashion similar to B-polarization, for C-polarization ($m = 1$) at $D = 19.5$, an asymmetric feature at 544 nm corresponding to the bonding and antibonding $l = 1$ dimer plasmons is visible. The antibonding $l = 2$ plasmon is also visible at 439 nm. For the shorter dimer separation $D = 3.0$ nm, four features are visible. These are the bonding and antibonding $l = 1$ plasmons at 558 and 533 nm and the bonding and antibonding $l = 2$ dimer plasmons at 458 and 435 nm.

As in the case for the homodimer, the extinction spectra of the heterodimers exhibit a strong polarization dependence when the dimer separation is small. The splittings between bonding and antibonding dimer plasmons and the shift of the dimer plasmons with dimer separation is smaller for the heterodimer than that for the homodimer. This is because the interaction between the nanoshells in the heterodimer is weaker because of the smaller size of one of the nanoshells.

D. Heterodimer Near Field. In this section, we investigate the near-field response of the heterodimer discussed in section 3.3. Figure 11 shows the field distributions of the heterodimer in a similar manner to Figures 5−7. The first, second, and third columns correspond to A-, B-, and C-polarization. The upper two rows in Figure 11 displays the field enhancements for wavelengths, corresponding to the two strongest features in the respective extinction spectra shown in Figure 10. The third row shows the electric field enhancements for the wavelength, corresponding to the dipole plasmon resonance maximum of the individual (39,48) nm nanoshell. Figure 11 clearly shows that for all polarizations, the strongest field enhancements occur for resonant excitation of the corresponding dimer plasmon modes.

The maximum field enhancement for the heterodimer system is for A-polarization with a value of 147. As with the

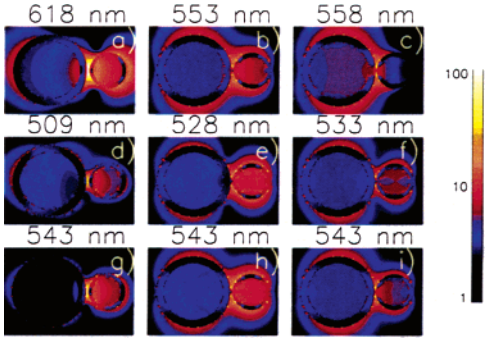

Figure 11. Near-field enhancements for a (39,48)−(19.5,24) nm Ag nanoshell heterodimer at specific resonant wavelengths for the three different incident field polarizations. The dimer separation is 3.0 nm. First column, for A-polarization; the second column, B-polarization; third column, C-polarization. The wavelengths for panels (a−f) corresponds to the two largest extinction maxima for each system. The wavelengths for (g−f) correspond to the dipolar plasmon resonance of the individual (39,48) nm nanoshell. Maximum field enhancements: (a) 147, (b) 21, (c) 35, (d) 42, (e) 17, (f) 14, (g) 68, (h) 22, and (i) 28.

homodimer, the location of the maximum electric field enhancement is at the center of the dimer junction and occurs when the incident wave is polarized parallel to the dimer axis. In panel (d) of Figure 11, the near-field pattern is a mixture of a dipole and quadrupole distributions. This clearly illustrates the mixing of plasmons of different angular momentum. For A- and B-polarizations, the bulk of the electric field enhancement is located in the vicinity of the smaller nanoshell of the dimer. This is in qualitative agreement with the findings from recent calculations of the near-field properties of self-similar nanolenses.[10] As in the homodimer case, the spatial distribution of the field enhancements for C-polarization depends strongly on the wavelength of the incident field. As the wavelength is increased from 450 to 580 nm (not shown), the location of the maximum field enhancements move continuously from the smaller to the larger nanoshell. Unlike the homodimer, the region between the nanoshells is always enhanced. This is due the fact that the magnitudes of the dipole moments on the constituent nanoshells are always different. As a result, the maximum enhancement for all polarizations of the heterodimer are larger than the maximum enhancement of the individual nanoshells.

IV. SERS

Nanoshells have been shown to be effective substrates for surface-enhanced Raman spectroscopy.[22,23] Nanoshells are very useful in SERS applications because they strongly enhance the local electric fields around their surfaces, and the wavelength at which this enhancement occurs is tunable. The electric field enhancement couples to the Raman cross section approximately as the fourth power.[40] In this subsection we will discuss the relevance of nanoshell dimers in SERS applications.

In Figure 12, we show the field enhancements of a nanoshell dimer as a function of dimer separation. For increasing dimer separation, the maximum field enhancement decreases; however, the volume within which the enhancements are significant also increases with increasing dimer separation. The strong field enhancements in the dimer junction for A-polarization result from the opposite alignment of the individual nanoshell plasmons and from the mixing (hybridization) of individual nanoparticle plasmons of higher angular momentum into the dimer plasmons. The reduction of the field enhancement with increasing dimer separation is a result of the increased separation of the surface charges of the individual nanoshells and the reduced

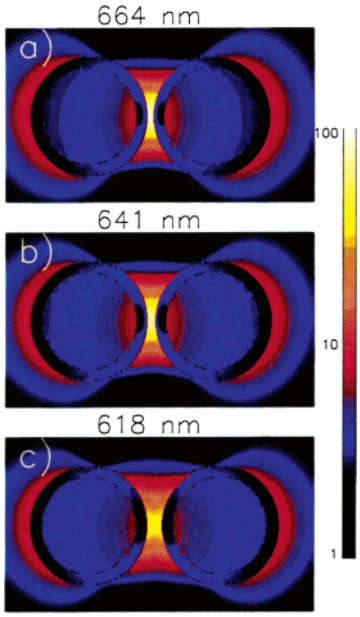

Figure 12. This figure shows a color contour plot of the near-field enhancements for a (39,48) nm Ag nanoshell homodimer for three different dimer separations: $D = 4.5$ nm (a), 6 nm (b), and 12 nm (c), illuminated with A-polarized light. The wavelengths correspond to maximum extinction, i.e., the excitation of the bonding $l = 1$ $m = 0$ dimer plasmons. The maximum field enhancements for the different dimer separations are 99 ($D = 4.5$ nm), 73 ($D = 6$ nm), and 38 ($D = 12$ nm).

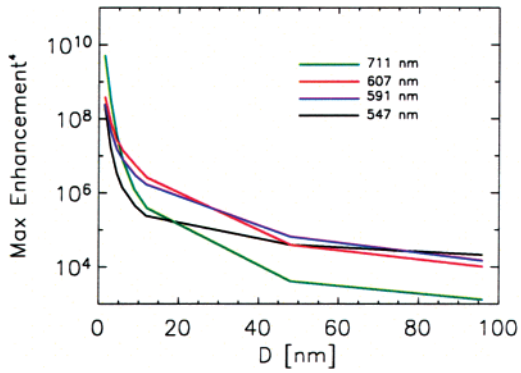

Figure 13. Calculated fourth power of the maximum electric field enhancement at the center of a nanoshell dimer junction as a function of dimer separation D for four different wavelengths. The incident light is a A-polarization. The dimer consists of two silver nanoshells of geometry (39,48) nm. The wavelengths corresponds to the $l = 1$ $m = 0$ dimer plasmons for dimer separations $D = 1.5$ (711 nm), 12 (607 nm), 24 (591 nm), and $D = \infty$ (isolated nanoshells).

coupling to the higher angular momentum plasmons of the individual nanoshells.

In Figure 13, we show the calculated maximum field enhancement in the dimer junction as a function of dimer separation for light incident with A-polarization for four different wavelengths. The wavelengths are chosen to correspond to the $l = 1$ $m = 0$ dimer plasmons for dimer separations $D = 1.5$, 12, 24 nm, and $D = \infty$. The figure illustrates the strong dependence of the maximum field enhancement on dimer separation. The plot shows that, for a molecule positioned at the center of the junction of a nanoshell dimer with $D = 1.5$ nm, the cross section for SERS would be increased by roughly 6 orders of magnitude compared to that of the enhancement for two isolated nanoshells.

Figure 13 reveals that the maximum field enhancement in the center of the nanoshell dimer junction is relatively insensitive

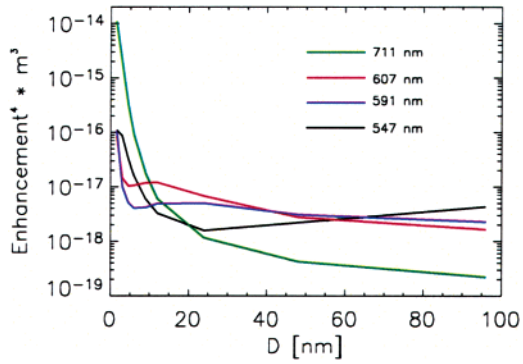

Figure 14. Calculated SERS efficiency of the maximum field enhancement at the center of a nanoshell dimer junction as a function of dimer separation D for four different wavelengths. We define the SERS efficiency as the integral of fourth power of the electric field enhancements in a volume within 0.75 nm outside the surfaces of the nanoshells. The incident light is of A-polarization. The dimer consists of two silver nanoshells of geometry (39,48) nm. The wavelengths corresponds to the $l = 1$ $m = 0$ dimer plasmons for dimer separations $D = 1.5$ (711 nm), 12 (607 nm), 24 nm (591 nm), and $D = \infty$ (isolated nanoshells).

to the wavelength of the incident light. This finding is consistent with the results in Figure 9, which show that the large field enhancements in the nanoshell dimer junction extends spectrally well outside the wavelength of the dimer plasmon resonance.

In a realistic nanoparticle Raman experiment, the target molecules would be distributed on the surfaces of the nanoparticle, not necessarily in the center of the dimer junction. Figure 12 shows that as the dimer separation increases, the volume of large field enhancements increases with dimer separation. The increased spatial extent of the region with large field enhancements makes the overall SERS efficiency of the dimer less dependent on the absolute value of the maximum field enhancements in the center of the junction.

To determine the effectiveness of nanoshell dimers as Raman sensors, we integrate the fourth power of the electric field enhancements in a volume within 0.75 nm outside the surfaces of one of the nanoshells as a function dimer separation for different wavelengths. By integrating over the shell surfaces, we account for both a random and a complete coverage of the target molecules. We will refer to this quantity as the SERS efficiency of the dimer. The four curves in Figure 14 are the SERS efficiency for the same wavelengths as in Figure 13. As in Figure 13, the integrated field enhancement increases with decreasing dimer separation. The SERS efficiency for $D = 1.5$ nm is approximately 3 orders of magnitude higher than that for the individual nanoshells. This is significantly smaller than what one would predict by only considering the maximum field enhancement at a single point, as in Figure 13. The maximum field at a particular point is generally an insufficient measure of SERS efficiency because the large field enhancements in the center of the dimer junction arise from a focusing effect, i.e., occurring at the expense of reduced field enhancements at other regions of the dimer. Such intense focusing may be relevant in single-molecule spectroscopy when the molecule can be appropriately positioned in the junction.

Figure 14 also shows a stronger wavelength dependence of the SERS efficiency of the dimer than what was apparent in Figure 13. The curves for wavelengths resonant with the dimer plasmons at dimer separations $D = 12$ nm and $D = 24$ nm display local maxima at these distances. For the wavelength corresponding to infinite separation, the SERS efficiency initially decreases with decreasing dimer separation because of the redshift of the dimer plasmon energy with decreasing dimer separation. Figure 14 clearly illustrates the importance of tuning the frequency of the incident light to the plasmon energies of the nanoparticle substrate. Only for the shortest dimer separations does the electromagnetic focusing effect of the nanoshell dimer balance the detuning of the plasmon resonance. For $D = 1.5$ nm, for all wavelengths considered, the SERS efficiency is at least an order of magnitude better than that for the individual nanoshells. The figure clearly shows that the SERS efficiency does not follow the fourth power of the maximum field enhancements in the center of the dimer junction.

V. Conclusions

In this paper, we have presented an application of the FDTD method to calculate the optical properties of metallic nanoshell dimers. The method was used to analyze the near- and far-field properties of nanoshell dimers both as a function of wavelength and as a function of incident field polarization. We found that both the extinction spectra of the dimer and its near-field enhancements depend strongly on polarization of the incident light and propagation direction of the incident wave with respect to the dimer orientation. The spatial variance of these enhancements with wavelength has been described, as well as the convergence of these results with mesh size. An analysis of the relevance of electric field enhancements for SERS revealed that, although the field enhancements in the dimer junction can be very significant, the spatial volume of the maximum enhancements is very small. Furthermore, the strong enhancements in the dimer junction occur at the expense of a reduced enhancement elsewhere around the dimer. An integration of the fourth power of the electric field enhancements around the surfaces of the dimer revealed that the SERS efficiency of the dimer is strongly dependent on wavelength of the incident light. Only if the frequency of the incident light is tuned to the dimer plasmon resonances will the dimer be significantly better as a SERS substrate than individual nanoshells.

Although the present study concerned nanoshell dimers, the qualitative aspects of the results are likely to apply also for nanosphere dimers. An extensive study of this system as well as of more general nanoshell heterodimers is in progress.

Acknowledgment. This work was supported by the Robert A. Welch Foundation under the grant C-1222, the Multi-University Research Initiative of the Army Research Office, and by the National Science Foundation under grants EIA-0216467, EEC-0304097, and ECS-0421108. It is a pleasure to acknowledge valuable discussions with D. Brandl, Dr. J. B. Jackson and Prof. N. J. Halas.

References and Notes

(1) Schatz, G. C.; Duyne, R. P. V. Electromagnetic Mechanism of Surface-enhanced Spectroscopy; In *Handbook of Vibrational Spectroscopy*; Chalmers, J. M., Griffiths, P. R., Eds.; John Wiley: Chichester, 2002; pp 1−16.

(2) Moskovits, M.; Tay, L.; Yang, J.; Haslett, T. *Top. Appl. Phys.* **2002**, *82*, 215−226.

(3) Kneipp, K.; Wang, Y.; Kneipp, H.; Perelman, L. T.; Itzkan, I.; Dasari, R. R.; Feld, M. S. *Phys. Rev. Lett.* **1997**, *78*, 1667−1670.

(4) Nie, S.; Emory, S. R. *Science* **1997**, *275*, 1102−1106.

(5) Michaels, A. M.; Nirmal, M.; Brus, L. E. *J. Am. Chem. Soc.* **1999**, *121*, 9932−9939.

(6) Wang, Z.; Pan, S.; Krauss, T. D.; Dui, H.; Rothberg, L. J. *Proc. Natl. Acad. Sci. U.S.A.* **2003**, *100*, 8638−8643.

(7) Markel, V. A.; Shalaev, V.; Stechel, E. B.; Kim, W.; Armstrong, R. L. *Phys. Rev. B* **1996**, *53*, 2425−2436.

(8) Stockman, M. I. *Phys. Rev. E* **1997**, *56*, 6494−6507.

(9) Kelly, K. L.; Coronado, E.; Zhao, L. L.; Schatz, G. C. *J. Phys. Chem. B* **2003**, *107*, 668−677.

(10) Li, K.; Stockman, M. I.; Bergman, D. J. *Phys. Rev. Lett.* **2003**, *91*, 227402−1−4.
(11) Aravind, P. K.; Nitzan, A.; Metiu, H. *Surf. Sci.* **1981**, *110*, 189−204.
(12) Schmeits, M.; Dambly, L. *Phys. Rev. B* **1991**, *44*, 12706−12712.
(13) Xu, H.; Bjerneld, E. J.; Kall, M.; Borjesson, L. *Phys. Rev. Lett.* **1999**, *83*, 4357−4360.
(14) Tamaru, H.; Kuwata, H.; Miyazaki, H. T.; Miyano, K. *Appl. Phys. Lett.* **2002**, *14*, 348−3492.
(15) Rechberger, W.; Hohenau, A.; Leitner, A.; Krenn, J. R.; Lamprecht, B.; Aussenegg, F. R. *Opt. Comm.* **2003**, *220*, 137−144.
(16) Su, K. H.; Wei, Q. H.; Zhang, X.; Mock, J. J.; Smith, D. R.; Schultz, S. *Nano Lett.* **2003**, *3*, 1087−1090.
(17) Futamata, M.; Maruyama, Y.; Ishikawa, M. *J. Phys. Chem. B* **2003**, *107*, 7607−7617.
(18) Prikulis, J.; Svedberg, F.; Kall, M.; Enger, J.; Ramser, K.; Goksor, M.; Hanstorp, D. *Nano Lett.* **2004**, *4*, 115−118.
(19) Wei, Q. H.; Su, K. H.; Durant, S.; Zhang, X. *Nano Lett.* **2004**, *4*, 1067−1071.
(20) Atay, T.; Song, J. H.; Nurmikko, A. V. *Nano Lett.* **2004**, *4*, 1627−1631.
(21) Moskovits, M.; Jeong, D. H. *Chem. Phys. Lett.* **2004**, *397*, 91−95.
(22) Jackson, J. B.; Westcott, S. L.; Hirsch, L. R.; West, J. L.; Halas, N. J. *Appl. Phys. Lett.* **2003**, *82*, 257−259.
(23) Jackson, J. B.; Halas, N. J. *Proc. Natl. Acad. Sci. U.S.A.* **2004**, *101*, 17930−17935.
(24) Jackson, J. B.; Halas, N. J. *J. Phys. Chem. B* **2001**, *105*, 2743−2746.
(25) Prodan, E.; Nordlander, P. *Nano Lett.* **2003**, *3*, 543−547.
(26) Prodan, E.; Nordlander, P.; Halas, N. J. *Nano Lett.* **2003**, *3*, 1411−1415.
(27) Prodan, E.; Radloff, C.; Halas, N. J.; Nordlander, P. *Science* **2003**, *302*, 419−422.
(28) Hao, E.; Li, S.; Bailey, R. C.; Zou, S.; Schatz, G. C.; Hupp, J. T. *J. Phys. Chem. B* **2004**, *108*, 1224−1229.
(29) Teperik, T. V.; Popov, V. V.; de Abajo, F. J. G. *Phys. Rev. B* **2004**, *69*, 155402.
(30) Grady, K.; Halas, N. J.; Nordlander, P. *Chem. Phys. Lett.* **2004**, *399*, 167−171.
(31) Oubre, C.; Nordlander, P. *J. Phys. Chem. B* **2004**, *108*, 17740−17747.
(32) Nordlander, P.; Oubre, C.; Prodan, E.; Li, K.; Stockman, M. I. *Nano Lett.* **2004**, *4*, 899−903.
(33) Wriedt, T. *Part. Part. Syst. Charact.* **1998**, *15*, 67−74.
(34) Taflove, A.; Hagness, S. C. *Computational Electrodynamics: The Finite-difference Time Domain Method*; Artech House: Norwood, MA, 2000.
(35) Sullivan, D. M. *Electromagnetic Simulation Using the FDTD Method*; IEEE Press: Piscataway, NJ, 2000.
(36) Johnson, P. B.; Christy, R. W. *Phys. Rev. B* **1972**, *6*, 4370.
(37) Nehl, C. L.; Grady, N. K.; Goodrich, G. P.; Tam, F.; Halas, N. J.; Hafner, J. H. *Nano. Lett.* **2004**, *4*, 2355−2359.
(38) Oubre, C.; Nordlander, P. *Proc. SPIE* **2003**, *5512*, 28−37.
(39) Prodan, E.; Nordlander, P. *J. Chem. Phys.* **2004**, *120*, 5444−5454.
(40) Kerker, M.; Wang, D.; Chew, H. *Appl. Opt.* **1980**, *19*, 4159−4174.